

See discussions, stats, and author profiles for this publication at: <https://www.researchgate.net/publication/233982923>

Antimicrobial and Biosensing Ultrasound-Responsive Lysozyme-Shelled Microbubbles

ARTICLE *in* ACS APPLIED MATERIALS & INTERFACES · DECEMBER 2012

Impact Factor: 6.72 · DOI: 10.1021/am302660j · Source: PubMed

CITATIONS

10

READS

45

7 AUTHORS, INCLUDING:



[Francesca Cavalieri](#)

University of Melbourne

65 PUBLICATIONS 1,361 CITATIONS

[SEE PROFILE](#)



[Subramanian Kaliappan](#)

University of Rome Tor Vergata

2 PUBLICATIONS 12 CITATIONS

[SEE PROFILE](#)



[Meifang Zhou](#)

University of Melbourne

30 PUBLICATIONS 444 CITATIONS

[SEE PROFILE](#)

Antimicrobial and Biosensing Ultrasound-Responsive Lysozyme-Shelled Microbubbles

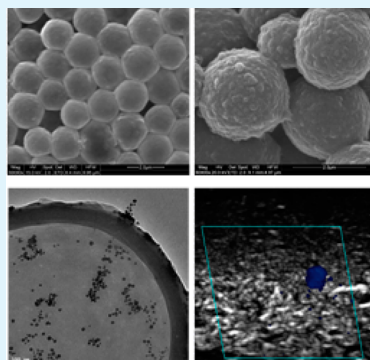
Francesca Cavalieri,^{*,†,‡} Laura Micheli,[†] Subramanian Kaliappan,[†] Boon M. Teo,[‡] Meifang Zhou,[‡] Giuseppe Palleschi,[†] and Muthupandian Ashokkumar^{*,‡}

[†]Dipartimento di Scienze e Tecnologie Chimiche, Università di Roma Tor Vergata, 00173 Roma, Italy.

[‡]School of Chemistry, The University of Melbourne, Parkville, Melbourne, Victoria 3010, Australia.

Supporting Information

ABSTRACT: Air-filled lysozyme microbubbles (LSMBs) were engineered as a support for the immobilization of gold nanoparticles and an enzyme, alkaline phosphatase, in order to develop micro-antimicrobial and biosensing devices. Gold nanoparticles immobilized on LSMBs significantly improved the antimicrobial efficacy of the microbubbles against *M. lysodeikticus*. The surface functionalization of the microbubbles with gold nanoparticles did not affect their echogenicity when exposed to an ultrasound imaging probe. Alkaline phosphatase was conjugated on the surface of microbubbles without compromising its enzymatic activity. The functionalized microbubbles were used for the detection of paraoxon in aqueous solutions.



KEYWORDS: microbubbles, lysozyme, gold nanoparticles, alkaline phosphatase, antimicrobial microparticles, biosensing microparticles

1. INTRODUCTION

Microbubbles (MBs) have enabled the development of new multifunctional agents for diagnostic imaging and drug delivery purposes.^{1,2} MBs are gas-filled colloidal particles with a size range between 0.5 and 10 μm , generally coated with a protein, lipid, or polymer^{3–5} layer. In the past, MBs have been used in clinical practice as ultrasound contrast agents in ultrasound myocardial perfusion imaging¹ and focal liver lesion diagnosis.⁶ They have been recently approved for the detection of focal breast lesions.⁷ During the past decade, MBs have been used as ultrasound responsive drug and gene delivery systems.^{1,2} The possibility to attach nanoparticles (NPs) and enzymes to MBs could be considered as a strategy to confer additional functionalities to MBs, such as antimicrobial and biosensing properties. Decoration of MBs' surface with magnetic or semiconductor NPs has been recently introduced for multimodal imaging.^{8,9} For example, quantum dot NPs can be used for optical imaging,⁸ gold nanorods can be used for photoacoustic imaging, and iron oxide or Gd-loaded NPs can be used for magnetic resonance imaging. MBs generated by a microfluidic method were incorporated with NPs, including CdSe/ZnS QDs, gold nanorods, iron oxide NPs and Gd-loaded mesoporous silica NPs.^{8–11} Particularly, gold nanoparticles (AuNPs) have attracted attention in the biomedical field due to their biocompatibility, facile conjugation to biomolecules and their unique optical properties conferred by their localized surface plasmon. AuNPs have been used as a bactericidal agent.^{12,13} Their predominant antimicrobial activity can be attributed to the cytotoxicity to various bacterial cells, i.e., they

can interact with the functional groups on the bacterial cell surface and inactivate bacteria.¹⁴ However, dispersed metallic NPs often tend to aggregate and separate from solutions, which results in a decrease of their antimicrobial efficiency. MBs provide a template on which gold NPs can be assembled and immobilized keeping the surface available for interaction with bacteria. We recently reported a simple method to synthesize stable and relatively monodisperse lysozyme nano- and microbubbles using sonication techniques.^{15,16} The micro-nanobubbles formed were found to possess echogenic properties resulting in 10 MHz ultrasound contrast imaging.¹⁷ The ultrasonic methodology^{18,19} constitutes a platform technique offering versatility in the synthesis of nano- and microbubbles, where the shell material can be a thiolated protein or polymer.²⁰ Numerous biomolecules such as proteins, polysaccharides and nucleic acids²¹ have been loaded to the lysozyme-shelled MBs, LSMBs, exploiting the hydrophobic/electrostatic/covalent interactions with the amines, carboxyl and thiols functional moieties of the protein. In addition, LSMBs are positively charged colloidal particles (ζ -potential $+40 \pm 3 \text{ mV}$)¹⁵ and provide a good template for the assembly of negatively charged NPs and biopolymers. We have shown that although lysozyme was partially denatured during the process of MB fabrication, LSMBs still possess significant antimicrobial activity.⁴ All these structural and functional

Received: November 11, 2012

Accepted: December 24, 2012

Published: December 24, 2012



features of LSMBs open up new opportunities for the development of novel multifunctional ultrasound responsive devices. Numerous examples of ligands conjugated MBs have been reported and in all cases decorated MBs are used for molecular imaging^{22,23} and targeted drug delivery.^{24–27} To the best of our knowledge, the development of powerful multi-functional MBs potentially applicable in food, health and environmental fields is still lacking. Herein, we report for the first time on the functionalization of LSMBs with bovine serum albumin, BSA-coated, and polyvinylpirrolidone(PVP)-coated AuNPs. The antimicrobial properties of LSMBs were evaluated after AuNPs were immobilized on MB surface.

In order to demonstrate a possible application of LSMBs as a biosensing device, LSMBs were engineered as a support for an enzyme, alkaline phosphatase (AP), and used for the detection of an analyte at very low concentrations. Particularly a new biosensing system for the determination of organophosphorous (OP)-based pesticides (paraoxon) in aqueous solution using covalently immobilized AP on LSMBs has been developed. OP-based pesticides, such as paraoxon, are the most widely used insecticides that can adversely affect the human nervous system even at low levels of exposure.^{28,29} Among enzymes suitable for the development of environmental bioassays, AP was selected as it is inhibited by organophosphate (OP)-based pesticides at ppb levels within a few seconds in aqueous solutions.³⁰ AP catalyzes the hydrolysis of phenyl phosphates to phenols. The enzyme is characterized by an activity at high pH, broad substrate specificity and uses a wide range of phosphomonoesters, such as *p*-nitrophenyl phosphate (uncolored) where the hydrolysis product is *p*-nitrophenol, yellow in color.³¹ The engineered system proposed in this work is an alternative method to the traditional^{32–34} technique (i.e., screen printed electrodes) used for the analysis of paraoxon, where the AP is conjugated to a colloidal system that can be easily recovered and reused by floatation.

2. EXPERIMENTAL SECTION

Materials. Tris buffer (tris(hydroxymethyl)amino methane), lysozyme from hen egg white, bovine serum albumin (BSA), polyvinylpirrolidone ($M_w = 30\,000$ Da), DL-dithiothreitol (DTT), tetrachloroauric acid, and *Micrococcus lysodeikticus* cells were purchased from Sigma-Aldrich (USA). Milli-Q filtered water ($18\,\Omega\text{cm}^{-1}$) was used to prepare all solutions. High-purity argon gas, provided by BOC gases, was used for purging solutions without further purification. The equipment employed for the sonochemical synthesis of gold nanoparticles comprising ELAK Nautik GmbH ultrasonic device (diameter of oscillator: 55 mm) operating at 213 kHz. A custom-made glass reaction cell was surrounded by a water jacket through which thermostatted water was circulated to maintain a constant temperature of 20 °C. The synthesis of LSMBs was carried out using a 20 kHz ultrasound generator (Branson) with a microtip (3 mm diameter horn) and adjustable power intensity.

Synthesis of Gold Nanoparticles. Gold nanoparticles stabilized by either PVP or BSA were synthesized using a sonochemical method. Specifically, 10 mL of aqueous tetrachloroauric acid, HAuCl₄ (0.4 mM) containing 3.7% (v/v) isopropanol and 0.5% (w/v) of PVP or 0.2% (w/v) of BSA was added to the reaction vessel and then purged with high-purity argon for 20 min. The gold nanoparticles synthesis experiments were carried out with at an ultrasonic frequency of 213 kHz at a constant ultrasonic power 0.6 W/mL, measured by calorimetry. During irradiation (up to 7 h), the reaction mixture was maintained at a constant temperature of 20 °C by circulating thermostatted water around the reaction vessel.

Synthesis and Functionalization of Lysozyme-Shelled Microbubbles, LSMB. LSMBs were synthesized as described previously.^{16,17} Lysozyme (5% w/v) was denatured in 50 mM Tris-

HCl (pH 8.3) buffer for 2 min using 120 mM DTT. A 3-mm diameter microtip of a high-intensity ultrasonic horn (20 kHz, Branson) was positioned at the air–water interface and operated at an acoustic power of 160 W cm⁻² for 30 s to obtain LSMBs. The mixture was then left standing for a few hours for LSMBs to float to the surface of the liquid. The excess DTT and the residual protein were repeatedly (5 times) washed off with Milli-Q water. 200 μL of the LSMB aqueous suspension with a bubble concentration of 1 mg mL⁻¹ was added to 30 μL of AuNP suspension and incubated for 24 h. The unreacted AuNPs were removed by LSMBs floatation and washing.

The determination of LSMB concentration was carried out using the BCA working reagent by BCA assay (Bicinchoninic Acid Kit for Protein determination - Sigma, Castle Hill, Australia) and standard lysozyme solution ranging from 5 mg mL⁻¹ to 0.02 mg mL⁻¹ and micro plate well; 0.24 mL of BCA working reagent (50 parts of BCA reagent A and 1 part of BCA reagent B) and 0.010 mL of standard solutions or LSMB suspension were added in each well. The microplate was placed in a spectrophotometer and the absorbance was measured at 570 nm. From the absorbance values, the concentration of LSMB was calculated using Sigma Plot 11.0 software. Determination of free thiol groups in lysozyme microspheres was carried out using Ellman's reagent prepared by dissolving 0.2 g of DTNB (*S,S'*-dithio-2-nitrobenzoate) in 50 mL of Tris buffer (pH 8), 6.9 g of glycine, and 1.2 g of EDTA; 2.8 mL of Tris buffer was added to 0.1 mL of Ellman's reagent and 0.1 mL of LSMB solution. The absorbance at 412 nm was then measured using UV spectrophotometer.

Characterization of Gold Nanoparticles and LSMBs. Transmission electron microscopy (TEM, FEI Tecnai F20) was used to image free gold nanoparticles and AuNPs on MB samples. Electron microscope specimens were prepared by placing drops of highly diluted samples on carbon coated grids and left to air-dry. UV-visible absorption spectra were obtained using a UV-vis spectrophotometer (Agilent 8453). A scanning electron microscope (SEM) (FEI Quanta) operated at an acceleration voltage of 15 kV was used to identify the morphology of the MBs. AFM images were taken using an MFP-3D Asylum Research Instrument in tapping mode on air-dried micro-capsules. A clinical sonography unit (Q Sonix) was used to examine the backscattering signals of lysozyme microbubbles (served as ultrasound contrast agents) and a phantom was used to mimic tissue structure. The phantom was made from gelatin and psyllium hydrophilic mucilloid fiber (Metamucil). The ultrasound applied on the phantom was 10 MHz with a mechanical index (MI) of 0.36.

Conjugation of Alkaline Phosphatase to LSMBs. The conjugation of AP to LSMBs to obtain LSMB-mAP was carried out as follows: 1 mg mL⁻¹ of MB and 0.5 mg mL⁻¹ of maleimide functionalized AP (m-AP) were allowed to react in 50 mM phosphate saline buffer at pH 7.2 for 15 min at room temperature under gentle stirring conditions. The reaction mixture was then purified by washing three times with Milli Q water. The LSMBs-mAP were recovered by floatation and the filtrate solutions were collected after each washing and analyzed to estimate the amount of unbound enzyme.

Determination of Enzymatic Activity of Maleimide-Activated Alkaline Phosphatase and LSMB-mAP. The enzymatic residual activity was determined with Boehringer Mannheim quality control assay, using *p*-nitrophenyl phosphate, as enzymatic substrate, in DEA buffer pH 9.8. The enzymatic substrate was hydrolyzed to *p*-nitrophenol by AP and detected spectrophotometrically at 405 nm within 10 min. The results were compared with that obtained with the same m-AP solution before the conjugation.

Preparation of a biosensing System Preparation for Paraoxon Monitoring. The functionalized LSMBs-mAP were employed as a biosensing system for the detection of paraoxon as a model compound in aqueous solutions. The degree of inhibition (inhibitor percentage, %I) of the paraoxon on the enzymatic activity of AP was measured as the relative decrease in absorbance observed after mixing LSMB-mAP and paraoxon. The absorbance of a LSMB-mAP suspension (1 mg mL⁻¹) in 1 M DEA was first measured by adding 1 mM of pNPP at room temperature under mild stirring condition. Subsequently 1 ppm of paraoxon (prepared in 1 M DEA) was added

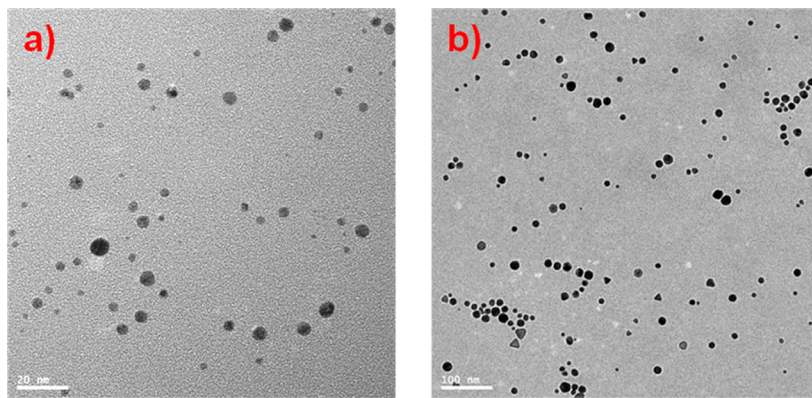


Figure 1. TEM images of (a) BSA-coated and (b) PVP-coated AuNPs.

to a fresh solution of LSMB-AP. The mixtures were incubated for 5 min and subsequently 1 mM of p-NPP was added. The %I was determined by the difference in absorbance before and after the addition of paraoxon: $\%I = [(A_0 - A_i)/A_0] \times 100$, where A_0 is the activity in the absence of inhibitor and A_i is activity in the presence of inhibitor. A calibration curve of paraoxon was prepared using 0, 0.5, 1, and 2 ppm of pesticide. The measurements were carried out in quartz cuvette at room temperature incubating the LSMB-AP in DEA buffer (1 mL) with several concentration of paraoxon. After 5 min, *p*-nitrophenyl phosphate was added to the solution. The absorbance measurements were carried out at 405 nm.

3. RESULTS AND DISCUSSION

Ultrasonic Synthesis of BSA- and PVP-Coated AuNP-Functionalized LSMBs. LSMBs were prepared as described previously.^{15,16} The mechanism responsible for the formation LSMBs is a combination of two ultrasound-induced phenomena: emulsification and oxidation. The emulsification of air bubbles induced by a 20 kHz horn in an aqueous protein solution creates a suspension of MBs and the aggregation of denatured lysozyme at the bubble/solution interface contributes to the stabilization of LSMBs. The protein shell is further stabilized by interprotein disulfide cross-linking of cysteine residues induced by the superoxide radicals generated during the sonolysis of water. The additional protein cross-linking via disulfide bridges significantly improved the microbubbles polydispersity and long-term stability for up to 1 year.

The diameter and shell thickness of LSMBs, measured by optical and scanning electron microscopy, are $2.5 \pm 0.5 \mu\text{m}$ and $150 \pm 50 \text{ nm}$, respectively.¹⁶ The residual and unreacted thiols on the shell of the microbubbles are available for functionalization with NPs and biomolecules. BSA- and PVP- coated AuNPs were prepared using an ultrasonic (213 kHz) synthetic method³⁵ without the use of external reducing agents. Au(III) in HAuCl₄ is reduced to AuNP by H⁺ and secondary radicals generated via acoustic cavitation. PVP was previously shown to be effective in stabilizing ultrasonically synthesized AuNPs.³⁵ BSA, the most abundant plasma protein, was recently used to generate Au(0) and stabilize Au particles of subnanometer to μm in dimensions.³⁶ The reducing ability of BSA, which may provide the electrons required for chloroaurate ion reduction, is generally exploited for the biominerallization of Au(III).^{37,38} Nevertheless the mild reducing power of BSA gives rise to slow reduction kinetics and consequently the reaction must be carried out for 24–48 h. Compared to these biominerallization synthetic approaches, the ultrasonic synthesis of BSA coated AuNP is a significantly faster and easier process. The absorption spectrum of synthesized AuNPs shows (Figure 1SI in the

Supporting Information) a single surface plasmon resonance band centered at 520 nm. The complete reduction of Au(III) and the formation of the BSA coated AuNPs were monitored by changes in the absorption spectra of the solution as a function of sonication time (inset Figure 1SI in the Supporting Information). The reaction was complete in 7 h. The formation of AuNPs was confirmed by transmission TEM, Figure 1. The BSA- and PVP- coated AuNPs are spherical in shape and have a diameter of $4.5 \pm 1 \text{ nm}$ and $15 \pm 5 \text{ nm}$, respectively.

The BSA- and PVP-coated AuNPs were stable and did not show aggregation up to 1 year. Both BSA and PVP act as steric stabilizers. BSA likely interacts with AuNPs by Au–S bonding via cysteine residues. The immobilization of AuNPs onto LSMB surface was achieved by incubating 200 μL of LSMB suspension (0.5 mg/mL) with 30 μL of AuNPs (0.4 mM) overnight as described in the Experimental Section. The presence of AuNPs on the surface of bubbles was verified by TEM, Figure 2a, suggesting large and evenly distributed adsorption of the small BSA coated AuNPs on LSMBs, whereas PVP coated AuNPs, Figure 2b, appear as organized clusters. The uptake of PVP- and BSA- coated AuNPs onto LSMBs (0.5 mg mL^{-1}) surface was quantified using UV-vis absorbance to be 14 and 25 μM , respectively. SEM (Figure 2d) images of LSMBs functionalized with AuNPs show a rougher surface compared to pristine LSMBs (Figure 2c). An AFM (Figure 2e) images of LSMBs functionalized with AuNPs is also shown. The deposition of AuNPs onto the surface of LSMBs' affected neither the size distribution nor the stability of microbubbles, which was monitored by bright-field optical microscopy.

The deposition of BSA-AuNPs onto the positively charged surface of LSMBs (ζ -potential +40 \pm 3 mV) slightly changed the ζ -potential of LSMBs to +34 \pm 2 mV, whereas the deposition PVP-AuNPs did not change the surface charge of LSMBs. Because of the very strong affinity of sulphydryl groups (SH) for gold surfaces, we can speculate that PVP- and BSA-coated AuNPs can interact with LSMBs by undergoing a ligand-exchange reaction³⁹ with the lysozyme thiols residing on LSMBs.

Antimicrobial Activity of LSMBs Functionalized with AuNPs. Lysozyme is an antimicrobial enzyme characterized by a single polypeptide chain and by enzymatic activity against the β -1,4 glycosidic bonds between *N*-acetylmuramic acid and *N*-acetylglucosamine, typical of bacteria peptidoglycans. Although lysozyme was partially denatured during the process of LSMB fabrication, the protein still possesses significant antimicrobial activity against *Micrococcus luteus*.¹⁵ In addition, we have

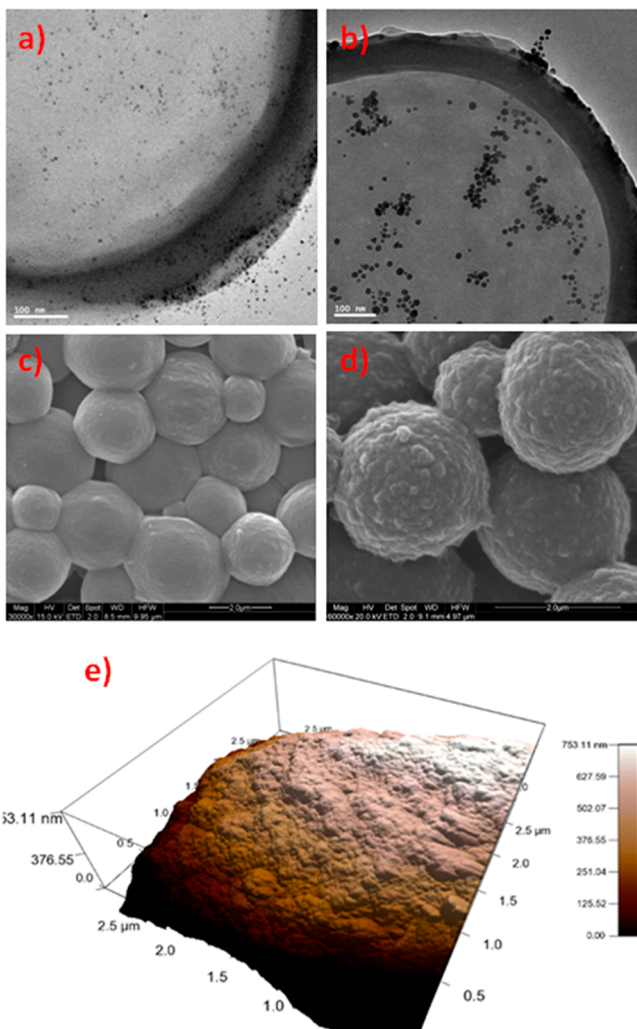


Figure 2. (a) TEM image of LSMBs functionalized with BSA-AuNPs; (b) TEM image of LSMBs functionalized with PVP-AuNPs; (c) SEM image of LSMBs; (d) SEM image of LSMBs functionalized with BSA-AuNPs; (e) AFM image of LSMB functionalized with BSA-AuNPs.

recently⁴ shown that LSMBs were able to interact with *Staphylococcus aureus* bacterial cells and inhibit biofilm formation in a concentration dependent manner. It is known that partially unfolded lysozyme is a bactericidal agent against both Gram-negative (*E. coli*) and -positive (*S. aureus*, *Micrococcus luteus*) bacteria regardless of its enzymatic muramidase activity.⁴⁰ The antimicrobial activity of partially unfolded lysozyme is attributed to the interaction of a hydrophobic pocket in the protein with bacterial cells leading to the disruption of the cell membranes. LSMBs' surface hydrophobicity and cationic properties can promote the interaction with the bacterial cell wall compromising its integrity and functions. Bacterial cell wall tends to attract positively charged LSMBs because of the total charge of the cell wall being negative. As a result, cell walls encounter high stress and LSMBs cause immediate cell lysis. A similar effect promoting rapid cell lysis was observed for polycations such as poly allylamine hydrochloride interacting with both Gram-positive and -negative bacteria.⁴¹ In addition, thiol groups present on the surface of LSMBs can interact with the functional groups on the surface of bacterial cell and inactivate the bacteria. Exofacial thiol groups are generally displayed by

membrane proteins or cell wall bound proteins⁴¹ to protect cells against oxidative stress. The capacity of functionalized LSMBs to induce bacterial cell lysis by breaking the peptidoglycans β -1,4 glycosidic bonds between N-acetylmuramic acid and N-acetylglucosamine was studied using turbidimetric method. The optical density of a suspension of *M. lysodeikticus* cells incubated with LSMBs (0.6 mg mL^{-1}) in 50 mM PBS decreased as a function of time.⁴² The initial slopes of the curves are correlated to the antimicrobial activity of the system. To ascertain the interaction nature of the functionalized LSMBs with bacteria, a comparison between the antimicrobial activities of the pristine LSMBs, AuNP-functionalized LSMBs and lactoferrin, Lf, coated LSMBs is discussed. Lf is an iron-glycoprotein in the innate immune system, which plays a relevant role in iron metabolism. We have demonstrated²¹ that adsorption of Lf layer onto the surface of LSMBs reverses the charge to $-7 \pm 1 \text{ mV}$ and likely buries the thiol groups available on the surface of LSMBs. The absence of antimicrobial activity for Lf functionalized LSMBs is shown in Figure 3. This

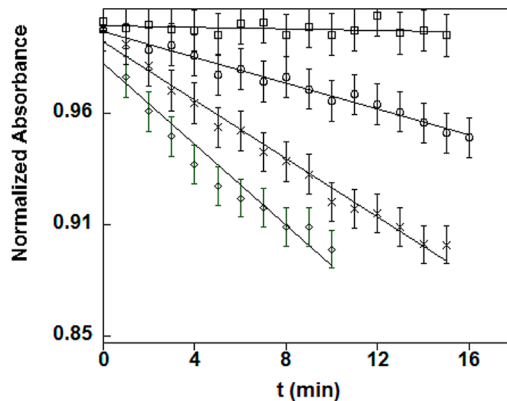


Figure 3. Antimicrobial activity of LSMBs (○), lactoferrin-coated LSMBs (□), BSA-AuNP-functionalized LSMBs (◊), and PVP-AuNP-functionalized LSMBs (×). The same concentration of LSMBs (0.6 mg mL^{-1}) was used for all assays.

result may be ascribed to both the negative surface charge and the inability of LSMBs to interact with bacteria via exofacial thiol groups. Interestingly, BSA- and PVP-coated AuNPs lack lysis activity against *M. lysodeikticus* within the observed time range (20 min). Conversely, both PVP- and BSA-coated AuNP immobilized on LSMBs significantly improved the antimicrobial efficacy against *M. lysodeikticus*. AuNPs could play a role in accelerating bacterial cell wall breakdown and cytoplasm release by acting as binding sites for bacteria and consequently increasing the interaction of *M. lysodeikticus* with the surface of LSMBs.

To determine the ultrasound backscattering ability of AuNPs coated LSMBs for imaging purposes, we used a 10 MHz scanner. We used a phantom as a tissue mimicking structure where a channel was made to flow the microbubble suspension. Lysozyme solution (1 mg mL^{-1}) was injected as a reference into the channel. Subsequently both pristine and AuNPs functionalized LSMB suspensions ($10^7 \text{ microbubbles mL}^{-1}$) were injected into the channel. The ultrasound probe was then used on the phantom at 10 MHz with a mechanical index (MI) at 0.36. The ultrasound scanning images show that the channel with lysozyme solution appears as a black hole (Figure 4a, d) showing no backscattering signal from the solution. Conversely pristine and gold functionalized LSMBs show a bright and blue

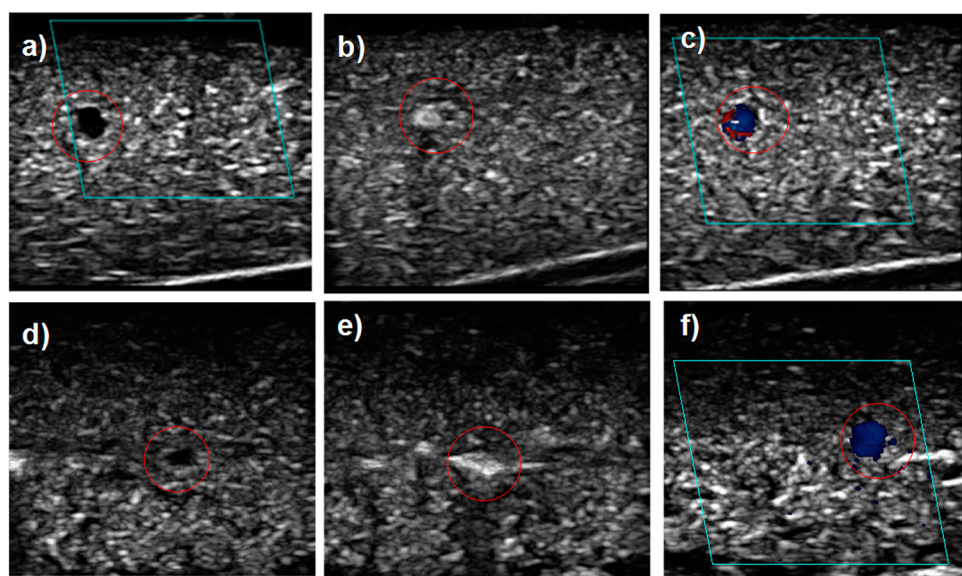
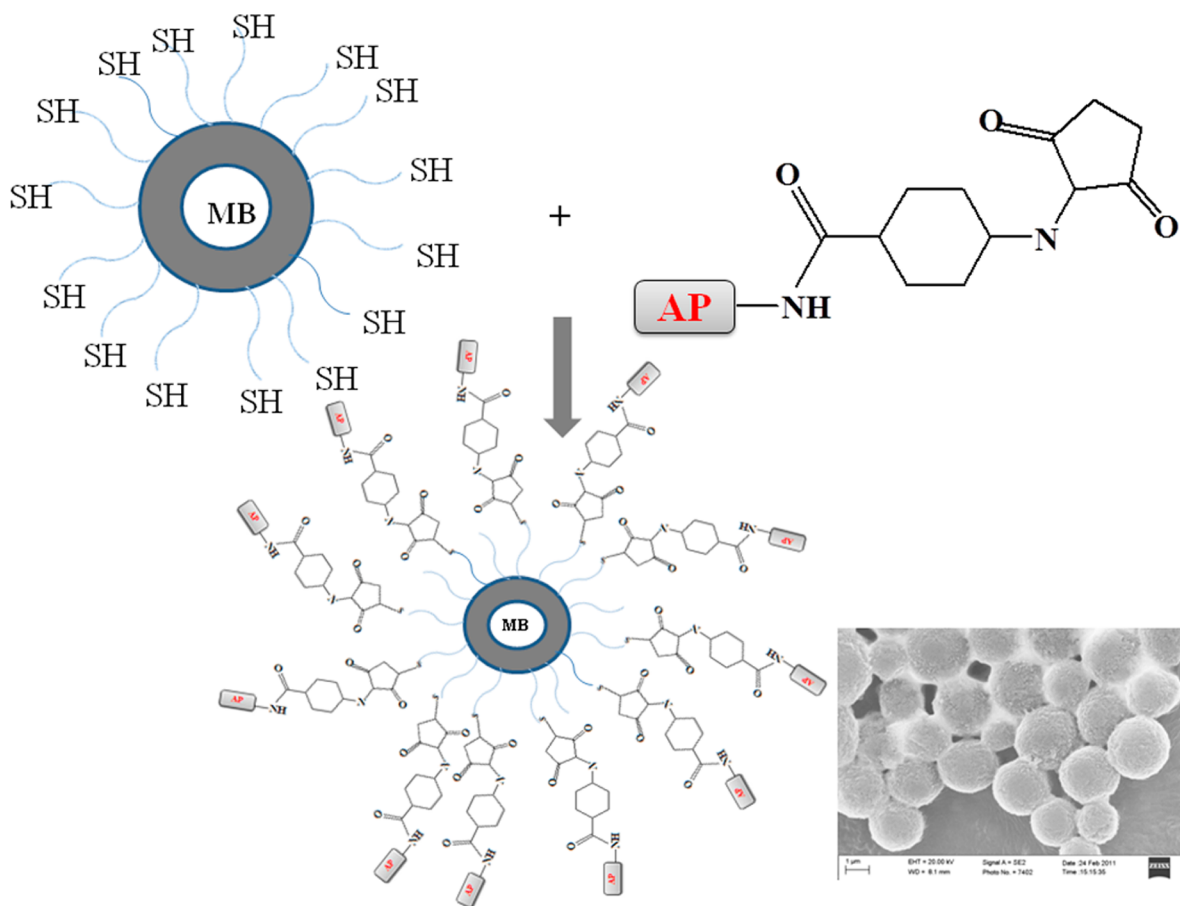


Figure 4. Ultrasound scanning images of (a, d) lysozyme aqueous solution, (b, c) pristine LSMBs solution (in (b) B mode and (c) Doppler mode), and (e, f) LSMBs functionalized with BSA- coated AuNPs (in (e) black mode and (f) color mode).

Scheme 1. Covalent Coupling of AP to the Preformed LSMBs



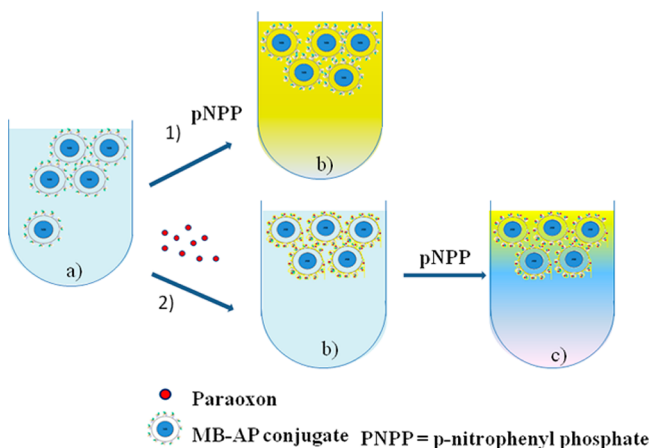
contrast within the hole (Figure 4b, 4e) under the B- mode and Doppler mode (Figure 4c, f). Contrast-enhanced ultrasound image of injected LSMB suspension was acquired up to 10 min. Thus, we have demonstrated that the functionalization of microbubbles with AuNPs does not affect their echogenicity under exposure to low-power US pulses.

Design of a Biosensor Using LSMBs Functionalized with AP. To demonstrate a possible application of LSMBs as a biosensing device, LSMBs were engineered as a support for AP and used for detection of paraoxon at very low concentrations. The developed method is a reversible assay relying on the capacity of the pesticide to compete with the substrate for

binding to enzyme, resulting in a partial inhibition of the enzymatic activity of AP. The extent of inhibition of the AP by paraoxon depends on the concentration of the inhibitor when the concentration of the substrate is kept constant. Covalent coupling of alkaline phosphatase to the preformed LSMBs was first accomplished using unreacted thiol groups that are present on the LSMB shell (Scheme 1).

We developed a protocol for the conjugation of AP based on maleamide functionalized AP (mAP) and thiol (-SH) groups present on the surface of LSMBs. The optimal conditions for conjugation reaction between mAP and LSMB (Scheme 2) to obtain LSMB-AP are detailed in the Experimental Section.

Scheme 2. Analysis of Paraoxon in Solution Using LSMB-AP



Different reaction conditions, such as the reaction time, amount of the reagent, stirring and pH of the buffer were tested. The conjugation procedure was optimized to avoid the aggregation of LSMBs. Optical microscopic analysis (data not shown) of LSMB-AP showed that the optimized conjugation procedure does not compromise the colloidal stability of microbubbles. The LSMB concentration was determined using a BCA protein assay. Boehringer Mannheim assay was used to assess the activity of the free and conjugated enzyme. Ellman's assay^{42,43} was used for the determination of residual free thiol groups before and after the conjugation reaction to determine the extent of conjugation. The results obtained from the conjugation reaction are shown in Table 1.

The yield of conjugation was 52% in terms of residual thiol (not coupled) groups on LSMBs. Since mAP bears single maleamide functionality a conjugation ratio of 17 mmol g⁻¹ was evaluated. This result suggests that not all thiol groups on the surface of LSMBs are accessible for AP conjugation as some of them are buried inside the protein shell.

The residual activity of enzyme present on the LSMB-AP was 57% in comparison to that of native enzyme (0.8 U/mL and 1.4 U/mL, respectively). This is a promising result considering that the commercially available conjugated enzyme kits typically

exhibit a 30–40% reduction in enzymatic activity.⁴⁴ The Michelis-Menten constant was calculated using “double-reciprocal” or Lineweaver–Burk plot⁴⁴ (Figure 5) to evaluate

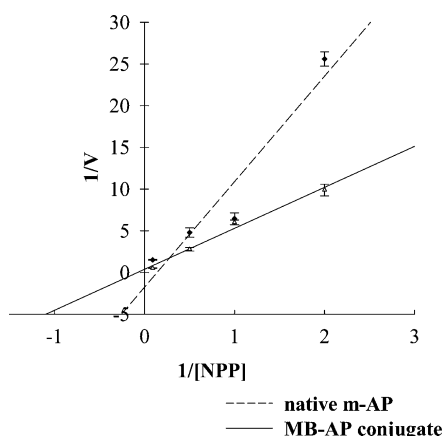


Figure 5. Lineweaver–Burk graph of NPP, substrate of alkaline phosphatase, in 1 M diethanolamine buffer (DEA), pH 9.8, containing 1 mM $\text{MgCl}_2 \cdot 6\text{H}_2\text{O}$.

whether the conjugation reaction had any effect on the affinity of the enzyme to its substrate, p-nitrophenyl phosphate (pNPP). Covalently conjugated and native enzyme exhibited K_m of 0.9 and 4.2 mM, respectively showing a decrease in the affinity for the conjugated enzyme. The presence of the enzyme covalently bonded on the LSMB surface is also confirmed by SEM images. From comparison of SEM images before (Figure 1c) and after conjugation (Scheme 1), the presence of AP aggregates on the surface of MBs can be clearly seen.

The AP aggregation may be responsible for the lower enzymatic activity as the binding sites could be covered by the protein clusters. Despite the fact that enzymatic activity of AP was reduced, the conjugation of AP on LSMB shell significantly improved the stability of the enzyme in Milli-Q water for up to 3 days. The possibility to use the AP-MB as a biosensing device was assessed by the evaluation of the enzymatic inhibition of LSMB-mAP induced by paraoxon.⁴⁵ The degree of inhibition (inhibitor percentage, %I) by paraoxon on the enzymatic activity of immobilized AP was measured as the relative decrease in absorbance following incubation of LSMB-AP with paraoxon (Scheme 2).

The mixtures were incubated for 5 min followed by the measurement of %I of the enzyme. The %I was determined by the difference in absorbance of the solution before and after the addition of paraoxon. The calibration curve for determination of paraoxon by using LSMB-AP conjugate is reported in Figure 6.

The decrease in absorbance is proportional to the concentration of the enzyme product and inversely proportional to that of the inhibitor. Also the extent of the inhibition was calculated by the difference in enzyme activity in the

Table 1. Conjugation Results in Terms of Free –SH Present on LSMBs, Residual Protein Concentration, and Enzyme Activity of AP before and after Conjugation with LSMBs

concentration of (mg mL ⁻¹) ^a		free –SH (mmol g ⁻¹ of MB)		enzyme activity (U/mL)	
native MB	MB conjugate	native MB	MB conjugate	native (m-AP)	MB conjugate
1.1 ± 0.2	0.59 ± 0.09	32.7 ± 0.3	15.7 ± 0.8	1.4 ± 0.03	0.80 ± 0.02

^aBCA using lysozyme as standard.

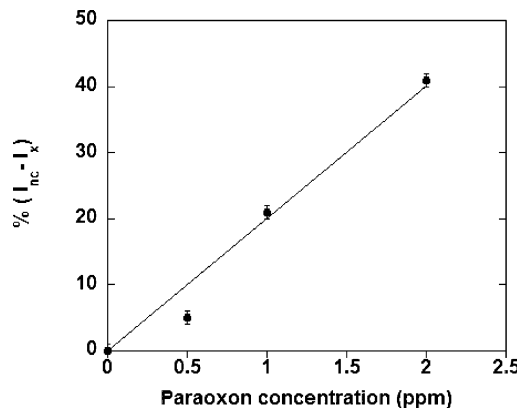


Figure 6. Calibration line for paraoxon; I_{nc} = Abs without inhibitor, I = Abs with inhibitor.

presence and absence of the inhibitor. A 20% competitive inhibition of enzyme activity, $\%I$, was observed for LSMB-AP conjugate incubated with 1 ppm paraoxon.

CONCLUSIONS

In summary, innovative applications of LSMBs have been successfully developed. LSMBs are a versatile platform for surface conjugation and functionalization with nanoparticles and biomolecules. LSMBs endowed with AuNPs exhibited a significant bactericidal activity and echogenic properties. A possible use as ultrasound responsive antimicrobial microdevice can be envisaged for this system. In addition, the successful conjugation of AP on LSMB surface resulted in a sensitive biosensor for the detection of analytes in aqueous solutions. These results pave the way for the engineering of new multifunctional LSMBs with a variety of uses in health, food, and environment related fields.

ASSOCIATED CONTENT

Supporting Information

Additional figures on ultrasonic synthesis of BSA-coated AuNPs. This material is available free of charge via the Internet at <http://pubs.acs.org>.

AUTHOR INFORMATION

Corresponding Author

*Phone +39 0672594461 (F.C.); +61383447090 (M.A.). Fax: +39 0672594328 (F.C.); +61-3-93475180 (M.A.). E-mail: francesca.cavalieri@uniroma2.it (F.C.); masho@unimelb.edu.au (M.A.).

Author Contributions

The manuscript was written through contributions of all authors. All authors have given approval to the final version of the manuscript.

Notes

The authors declare no competing financial interest.

ACKNOWLEDGMENTS

This work was supported by European Project IRSES Marie Curie, the University of Melbourne IPRS fellowship, and Victorian Government VIRS fellowship.

ABBREVIATIONS

LSMBs, lysozyme-shelled microbubbles; AuNPs, gold nanoparticles

REFERENCES

- Cosgrove, D.; Harvey, C. *Med. Biol. Eng. Comput.* **2009**, *47*, 813–826.
- Ferrara, K.; Pollard, R.; Borden, M. *Annu. Rev. Biomed. Eng.* **2007**, *9*, 415–447.
- Sirsi, S.; Borden, M. *Bubble Sci. Eng. Technol.* **2009**, *1*, 3–17.
- Cavalieri, F.; Zhou, M.; Tortora, M.; Baldassarri, L.; Ashokkumar, M. *Curr. Pharm. Des.* **2012**, *18*, 2135–2151.
- Cavalieri, F.; Zhou, M.; Ashokkumar, M. *Curr. Top. Med. Chem.* **2010**, *12*, 1198–1210.
- Blomley, M. J.; Albrecht, T.; Cosgrove, D. O.; Patel, N.; Jayaram, V.; Butler-Barnes, J.; Eckersley, R. J.; Bauer, A.; Schlieff, R. *Radiology* **1999**, *210*, 409–416.
- Hongjia, Z.; Rong, X.; Qifang, O.; Lidian, C.; Baowei, D.; Ye, H. *Eur. J. Radiat.* **2010**, *73*, 288–293.
- Park, J. I.; Jagadeesan, D.; Williams, R.; Oakden, W.; Chung, S.; Stanisz, G. J.; Kumacheva, E. *ACS Nano* **2010**, *4*, 6579–6586.
- Seo, M.; Gorelikov, I.; Williams, R.; Matsuura, N. *Langmuir* **2010**, *26*, 13855–13860.
- Yang, F.; Zhang, M.; He, W.; Chen, P.; Cai, X.; Yang, L.; Gu, N.; Wu, J. *Small* **2011**, *7*, 902–910.
- Yang, F.; Li, Y.; Chen, Z.; Zhang, Y.; Wu, J.; Gu, N. *Biomaterials* **2009**, *30*, 3882–3890.
- Zhao, Y.; Tian, Y.; Cui, Y.; Liu, W.; Ma, J.; Jiang, X. *J. Am. Chem. Soc.* **2010**, *132*, 12349–12356.
- Zhou, Y.; Kong, Y.; Kundu, S.; Cirillo, J. D.; Liang, H. *J. Nanobiotechnol.* **2012**, *10*, 10–19.
- Biradar, D.; Lingappa, K.; Dayanand, A. *J. Ecobiotechnol.* **2012**, *4*, 43–45.
- Cavalieri, F.; Ashokkumar, M.; Grieser, F.; Caruso, F. *Langmuir* **2008**, *24*, 10078–10083.
- Zhou, M.; Cavalieri, F.; Ashokkumar, M. *Soft Matter* **2011**, *7*, 623–630.
- Zhou, M.; Cavalieri, F.; Caruso, F.; Ashokkumar, M. *ACS Macro Lett.* **2012**, *1*, 853–856.
- Suslick, K. S.; Grinstaff, M. W. *J. Am. Chem. Soc.* **1990**, *112*, 7807–7809.
- Dibbern, E. M.; Toublan, F. J.-J.; Suslick, K. S. *J. Am. Chem. Soc.* **2006**, *128*, 6540–6541.
- Cavalieri, F.; Zhou, M.; Caruso, F.; Ashokkumar, M. *Chem Comm.* **2012**, *47*, 4096–4098.
- Melino, S.; Zhou, M.; Tortora, M.; Paci, M.; Cavalieri, F.; Ashokkumar, M. *Amino Acids* **2012**, *43*, 885–896.
- Klibanov, A. L. *Invest. Radiol.* **2006**, *41*, 354–362.
- Kiessling, F.; Huppert, J.; Palmowski, M. *Curr. Med. Chem.* **2009**, *16*, 627–642.
- Klibanov, A. L. *Bioconjugate Chem.* **2005**, *16*, 9–17.
- Treat, L. H.; McDannold, N.; Vykhodtseva, N.; Zhang, Y.; Tam, K.; Hyynnen, K. *Int. J. Cancer* **2007**, *121*, 901–907.
- Rapoport, N. Y.; Kennedy, A. M.; Shea, J. E.; Scaife, C. L.; Nam, K.-H. *J. Controlled Release* **2009**, *138*, 268–276.
- Richman, M.; Wilk, S.; Skirtenko, N.; Perelman, A.; Rahimipour, S. *Chemistry* **2011**, *26*, 11171–11177.
- Chapalamadugu, S.; Chaudhry, S. S. *Crit. Rev. Biotechnol.* **1992**, *12*, 357–389.
- FAO *Production Yearbook* 1989; Food and Agricultural Organization of United Nations (FAO): Rome, 1989; Vol. 43, p 320.
- Ayyagari, M.; Kamtekar, P. R. S.; Gai, H.; Marx, K. A.; Kumar, J.; Tripathy, S. K. *Biotechnol. Bioeng.* **1995**, *45*, 116–121.
- Millán, J. L. *Purinergic Signalling* **2006**, *2*, 335–341.
- Aprea, C.; Colosio, C.; Mammone, T.; Minoia, C.; Maroni, M. *J. Chromatogr., B* **2002**, *769*, 191–219.
- Amine, A.; Mohammadi, H.; Bourais, I.; Palleschi, G. *Biosens. Bioelectron.* **2006**, *21*, 1405–1423.
- Arduini, F.; Ricci, F.; Tuta, C. S.; Moscone, D.; Amine, A.; Palleschi, G. *Anal. Chim. Acta* **2006**, *580*, 155–162.
- Okitsu, K.; Ashokkumar, M.; Grieser, F. *J. Phys. Chem. B* **2005**, *109*, 20673–20675.

- (36) Liu, H.; Zhang, X.; Wu, X.; Jiang, L.; Burda, C.; Zhu, J. *J. Chem. Commun.* **2011**, *47*, 4237–4239.
- (37) Xie, J.; Lee, J. Y.; Wang, D. I. C. *J. Phys. Chem. C* **2007**, *111*, 10226–10232.
- (38) Xie, J.; Zheng, Y.; Ying, J. Y. *J. Am. Chem. Soc.* **2009**, *131*, 888–889.
- (39) Carotenuto, G.; Nicolais, L. *J. Mater. Chem.* **2003**, *13*, 1038–1041.
- (40) Ibrahim, H.; Higashiguchi, S.; Koketsu, M.; Juneja, L. R.; Kim, M.; Yamamoto, T.; Sugimoto, Y.; Aoki, T. *J. Agric. Food. Chem.* **1996**, *44*, 3799–30806.
- (41) Lichten, J. A.; Rubner, M. F. *Langmuir* **2009**, *7*, 7686–7694.
- (42) Michelon, D.; Abraham, S.; Ebel, B.; De Coninck, J.; Husson, F.; Feron, G.; Gervais, P.; Cachon, R. *FEBS J.* **2010**, *277*, 2282–2290.
- (43) Ellman, G. L. *Arch. Biochem. Biophys.* **1959**, *82*, 70–77.
- (44) Neagu, D.; Micheli, L.; Palleschi, G. *Anal. Bioanal. Chem.* **2006**, *385*, 1068–1074.
- (45) Jenkis, W. T.; D'Ari, L. *J. Biol. Chem.* **1966**, *241*, 295–296.